Assessment of cyclooxygense-2 expression with ^{99m}Tc-labeled celebrex

David J. Yang[a], Jerry Bryant[a], Joe Y. Chang[b], Richard Mendez[a], Chang-Sok Oh[a], Dong-Fang Yu[a], Megumi Ito[a], Ali Azhdarinia[a], Sahar Kohanim[a], E. Edmund Kim[a], Edward Lin[c] and Donald A. Podoloff[a]

Cyclooxygenase-2 (COX-2) plays an important role in angiogenesis and cancer progression. Since many tumor cells exhibit COX-2 expression, functional imaging of COX-2 expression using celebrex (CBX, a COX-2 inhibitor) may provide not only a non-invasive, reproducible, quantifiable alternative to biopsies, but it also greatly complements pharmacokinetic studies by correlating clinical responses with biological effects. Moreover, molecular endpoints of anti-COX-2 therapy could also be assessed effectively. This study aimed at measuring uptake of ^{99m}Tc-EC–CBX in COX-2 expression in tumor-bearing animal models. *In vitro* Western blot analysis and cellular uptake assays were used to examine the feasibility of using ^{99m}Tc-EC–CBX to measure COX-2 activity. Tissue distribution studies of ^{99m}Tc-EC–CBX were evaluated in tumor-bearing rodents at 0.5–4 h. Dosimetric absorption was then estimated. Planar scintigraphy was performed in mice, rats and rabbits bearing tumors. *In vitro* cellular uptake indicated that cells with higher COX-2 expression (A549 and 13762) had higher uptake of ^{99m}Tc-EC–CBX than lower COX-2 expression (H226). *In vivo* biodistribution of ^{99m}Tc-EC–CBX in tumor-bearing rodents showed increased tumor:tissue ratios as a function of time. *In vitro* and biodistribution studies demonstrated the possibility of using ^{99m}Tc-EC–CBX to assess COX-2 expression. Planar images confirmed that the tumors could be visualized with ^{99m}Tc-EC–CBX from 0.5 to 4 h in tumor-bearing animal models. We conclude that ^{99m}Tc-EC–CBX may be useful to assess tumor COX-2 expression. This may be useful in the future for selecting patients for treatment with anti-COX-2 agents. *Anti-Cancer Drugs* 15:255–263 © 2004 Lippincott Williams & Wilkins.

Anti-Cancer Drugs 2004, **15**:255–263

Keywords: COX-2 imaging, ^{99m}Tc-EC–celebrex

Divisions of [a]Diagnostic Imaging, [b]Radiation Oncology and [c]Cancer Medicine, University of Texas M. D. Anderson Cancer Center, Houston, TX, USA.

Correspondence to D. J. Yang, Department of Nuclear Medicine, University of Texas M. D. Anderson Cancer Center, 1515 Holcombe Boulevard, Houston, TX 77030, USA.
Tel: +1 713 794-1053; fax: +1 713 794-5456;
e-mail: dyang@di.mdacc.tmc.edu

Received 8 November 2003 **Accepted** 24 November 2003

Introduction

Epidemiological studies have shown that non-steroidal anti-inflammatory drugs (NSAIDs) such as aspirin significantly reduce the risk of colorectal, esophageal, gastric, lung and breast cancers. NSAIDs inhibit prostaglandin endoperoxide synthase [cyclooxygenase (COX)] activity. This enzyme introduces two molecules of O_2 into arachidonic acid to form prostaglandin (PG) G_2, which is then reduced to PGH_2. PGH_2 is converted to PGE_2, $PGF_{2\alpha}$, PGI_2 and thromboxanes by separate enzymes [1–3]. PGs are critical mediators of physiologic processes and inflammation. They are produced by two different isoforms of the COX enzyme, i.e. COX-1 and COX-2. In particular, COX-2 was demonstrated to be crucial for PG synthesis in inflammation, and its concentrations are elevated in the epithelial cells within human colorectal, esophageal, head and neck, and lung cancers. Although COX-1 is considered a housekeeping gene in most tissues, COX-1 is constitutively expressed in most tissues, with highest levels found in the stomach, platelets, renal tubules and liver. COX-1 produces PGs necessary for normal physiologic functions, e.g. maintaining the integrity of the gastrointestinal tract and platelet function. The COX-1 gene may also be important in temperature regulation and in mediating the pyresis that occurs in the absence of infection [4,5]. In contrast, COX-2 is not expressed in normal tissues; however, it is greatly induced during inflammation or tumorigenesis [6].

Specific COX-2 inhibitor such as celecoxib [celebrex (CBX)] spare COX-1 inhibition associated with NSAIDs which induced peptic ulcer disease, reduced platelet function and renal tubule toxicity. Celecoxib, a specific COX-2 inhibitor, was approved for osteoarthritis or rheumatoid arthritis based on its potent anti-inflammatory activity and favorable toxicity profile with a reduced incidence of peptic ulcer [7]. Inhibition of COX-2 by celecoxib delays tumor growth and metastasis in xenograft tumor models as well as suppresses basic fibroblast growth factor 2-induced neovascularization of the rodent cornea. In addition, celecoxib, given daily in the diet,

0959-4973 © 2004 Lippincott Williams & Wilkins DOI: 10.1097/01.cad.0000119732.04668.6d

significantly inhibited the induction of rat mammary tumors by 7,12-dimethylbenz[*a*]anthracene [7]. These results indicate that celecoxib has significant antineoplastic activity. Non-invasive molecular imaging of COX-2 expression *in vivo* would be useful to assess clinical endpoints in validating the COX-2 response with anti-COX-2-based clinical studies.

Due to favorable physical characteristics as well as extremely low cost, ^{99m}Tc has been preferred for labeling radiopharmaceuticals. Several compounds have been labeled with ^{99m}Tc using nitrogen and sulfur chelates [8,9]. Bis-aminoethanethiol tetradentate ligands, also called diaminodithiol compounds, are known to form very stable Tc(V)O complexes on the basis of efficient binding of the oxotechnetium group to two thiolsulfur and two amine nitrogen atoms. ^{99m}Tc-L,L-ethylenedicysteine (^{99m}Tc-EC) is a recent and successful example of N_2S_2 chelates [10,11]. EC can be labeled with ^{99m}Tc easily and efficiently with high radiochemical purity and stability and is excreted through the kidneys by active tubular transport [12,13]. A series of ^{99m}Tc-EC–agent conjugates for functional imaging in oncology have been previously reported [14–21]. EC–agent conjugates provide minimal structural alteration. In this paper, tumor uptake of ^{99m}Tc-EC–celebrex in various cell lines, and biodistribution and planar imaging in tumor-bearing animal models are presented.

Materials and methods

Chemicals and analysis

Mass spectral analyses were conducted at the University of Texas Health Science Center (Houston, TX). NMR spectra were recorded on a Bruker 500 Spectrometer. The mass data were obtained by fast atom bombardment on a Kratos MS 50 instrument. *N*-hydroxysulfosuccinimide (Sulfo-NHS) and 1-ethyl-3-(3-dimethylaminopropyl) carbodiimide–HCl (EDC) were purchased from Pierce (Rockford, IL). All other chemicals were purchased from Aldrich (Milwaukee, WI). Celebrex capsules (Pfizer, New York, NY) were obtained from M. D. Anderson Hospital Pharmacy. [^{18}F]FDG was purchased from PET NET (Houston, TX). Silica gel-coated thin-layer chromatography (TLC) plates were purchased from Whatman (Clifton, NJ).

Synthesis of EC

EC was prepared in a two-step synthesis according to the previously described methods [10,11]. Briefly, cysteine–HCl (41.52 g) was dissolved in water (106 ml). To this, formaldehyde was added (26.1 ml) and the reaction mixture was stirred overnight at room temperature. Pyridine (26.6 ml) was then added and the precipitate formed. The crystals were separated and washed with ethanol (54 ml) for 25 min at room temperature, then filtered with a Buchner funnel. The crystals were triturated with petroleum ether (150 ml), again filtered and then lyophilized for 3 days. The precursor, L-thiazolidine-4-carboxylic acid (m.p. 195°C, reported 196–197°C), was used for synthesis of EC. The precursor (22 g) was dissolved in liquid ammonia (200 ml) and refluxed. Sodium metal was added until a persistent blue color appeared. Ammonium chloride was added to the blue solution and then the solvents were evaporated to dryness. The residue was dissolved in water (200 ml) and the pH was adjusted to 2. A precipitate formed, and was filtered and washed with water (500 ml). The solid (EC) was dried in a calcium chloride dessicator and weighed 10.7 g (48.2% yield, m.p. 247°C, reported 251–253°C). The structure was confirmed by ^{1}H-NMR and fast-atom bombardment mass spectroscopy (FAB-MS).

Synthesis of ethylamino COX-2 (EA–CBX)

N-4-(5-*p*-tolyl-3-trifluoromethyl-pyrazol-1-yl)benzenesulfonylamide (CBX) was extracted from celebrex capsules. Briefly, whole capsule contents were suspended in chloroform. The mixture was filtered and the chloroform layer was evaporated to dryness, yielded crude CBX product. CBX (114.4 mg, 0.3 mmol) was dissolved in chloroform (2 ml). To this solution, DBU 44.9 µl (0.3 mmol in chloroform 0.5 ml) and ethyl isocyanatoacetate 33.7 µl (0.3 mmol in chloroform 0.5 ml) were added. The reaction was stirred at room temperature for 6 h. The solvent was evaporated *in vacuo*. The product was isolated from a silica gel-packed column using chloroform/methanol as an eluant. The yield of the ester form of CBX (compound **I**) was 135 mg (88.1%). The synthetic scheme is shown in Figure 1. NMR spectra data of compound **I** is shown in Figure 2. Compound **I** (102 mg, 0.2 mmol) was then dissolved in 2 ml of methanol and ethylene diamine (72.9 µl) was added. The reaction was stirred at room temperature for 24 h. The product was isolated from silica gel-packed column using chloroform:methanol as an eluant. The desired EA–CBX (compound **II**) was isolated (91 mg, 86.7% yield). NMR spectra data of compound **II** is shown Figure 3.

Synthesis of EC–ethylamino CBX conjugate (EC–CBX)

To dissolve EC, NaOH (1 N, 0.6 ml) was added to a stirred solution of EC (42.3 ma, 0.15 mmol) in water (3 ml). To this colorless solution, Sulfo–NHS (65.1 mg, 0.3 mmol) and EDC (57.5 mg, 0.3 mmol) were added. EA-CBX (78.6 mg, 0.15 mmol) was then added. The mixture was stirred at room temperature for 24 h. The mixture was dialyzed for 48 h using a Spectra/POR molecular porous membrane with molecule cut–off at 500 (Spectrum Medical Industries, Houston, TX). After dialysis, the product was dried under lyophilization. The product weighed 87.5 mg (yield 75%). NMR spectra data of EC–CBX is shown in Figure 4.

Fig. 1

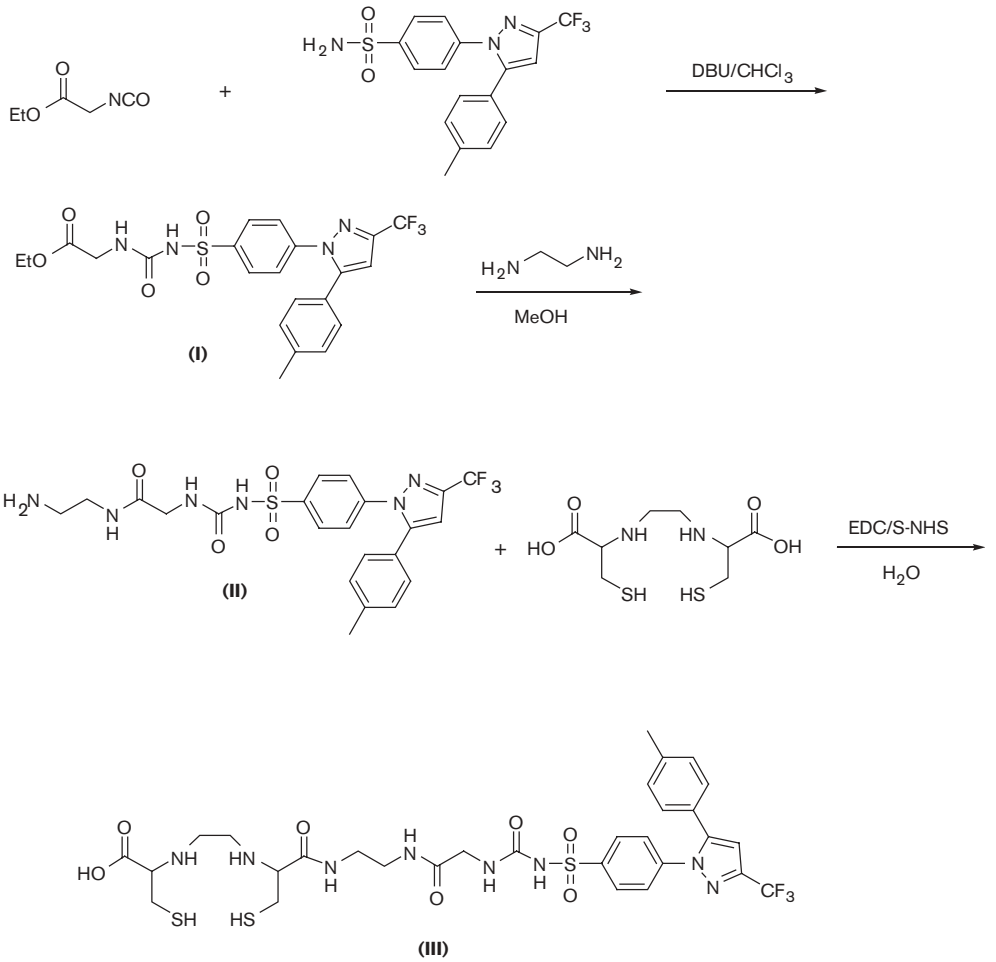

Synthetic scheme of EC–CBX.

Radiolabeling of EC–CBX with ^{99m}Tc

Radiosynthesis of ^{99m}Tc–EC–CBX was achieved by adding required amount of [^{99}mTc]pertechnetate into a home–made kit containing the lyophilized residue of EC–CBX (5 mg), $SnCl_2$ (100 μg), Na_2HPO_4 (13.5 mg), ascorbic acid (0.5 mg), glutamic acid (2 mg) and EC (0.5 mg). Final pH of the preparation was 7.4. Radiochemical purity was determined by TLC (ITLC SG; Gelman Sciences, Ann Arbor, MI) eluted with, respectively, ammonium acetate (1 M in water):methanol (4:1). From radio–TLC (Bioscan, Washington, DC) analysis, the radiochemical purity was $> 95\%$.

In vitro cellular uptake studies

To evaluate if the uptake of ^{99m}Tc-EC–CBX correlates to COX-2 expression, *in vitro* cellular uptake assay was conducted using high, intermediate and low COX-2-expressing cancer cell lines 13762 (breast), A549 (lung) and H226 (lung), respectively. H226 was known to have lower COX-2 expression than A549 [22,23]. However, little was known about 13762 rat-driven breast tumor cells, thus Western blot analysis was performed on 13762 and A549 (positive control) cancer cells. Cancer cells were treated with celebrex (10 μg) and then lysed with buffer containing 20% SDS in dimethyl formamide/H_2O, pH 4.7, at 37°C. The supernatants were cleared by centrifugation and the protein concentrations were measured by the Lowry method. Equal amounts of protein were subjected to immunoprecipitation in the presence of mouse anti-human COX-2 antibody (Santa Cruz Biotechnology, San Diego, CA) for 2 h at 4°C, followed by incubation with immobilized Protein G Plus/Protein A–agarose beads (Oncogene Research Products, Cambridge, MA) overnight at 4°C. For Western immunoblotting, the immunoprecipitates or equal amounts of crude extract were boiled in Laemmli SDS sample buffer, resolved by SDS–PAGE, transferred to nitrocellulose and probed with mouse antiphosphorylation primary antibody (Upstate Biotechnology, Lake Placid, NY) at 4°C overnight. After the blots were incubated for another 1 h at

Fig. 2

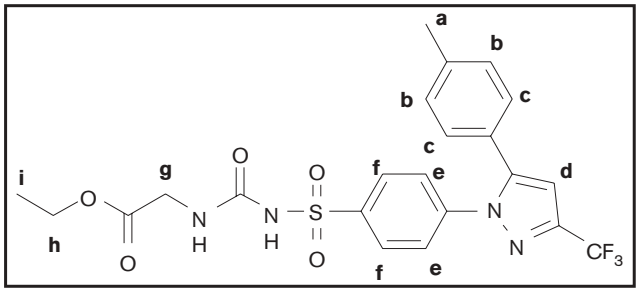

Observed (p.p.m.)

7.86 (2H, d, *J*=8.6Hz)	**f**
7.33 (2H, d, *J*=8.6Hz)	**e**
7.03 (2H, d, *J*=8.2Hz)	**c**
6.98 (2H, d, *J*=8.2Hz)	**b**
6.62 (1H, s)	**d**
4.41 (2H, s)	**g**
4.01 (2H, q, *J*=7.1Hz)	**h**
2.22 (3H, s)	**a**
1.11 (3H, t, *J*=7.1Hz)	**I**

^{1}H-NMR spectra data of ester analog of celebrex (compound **I**).

Fig. 3

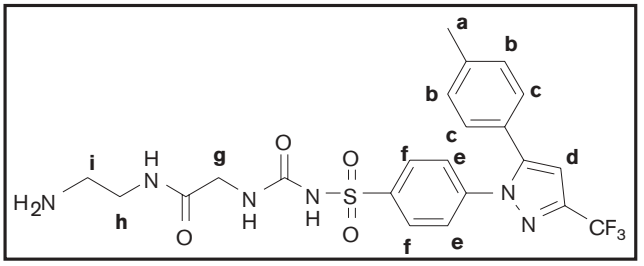

Observed (p.p.m.)

7.83 (2H, d, *J*=8.6Hz)	**f**
7.27 (2H, d, *J*=8.6Hz)	**e**
7.03–7.09 (4H, m)	**c,b**
6.68 (1H, s)	**d**
3.56 (2H, br)	**g**
3.38 (2H, br)	**h**
2.94 (2H, br)	**I**
2.26 (3H, s)	**a**

^{1}H-NMR spectra data of ethylenediamine analog of celebrex (compound **II**).

Fig. 4

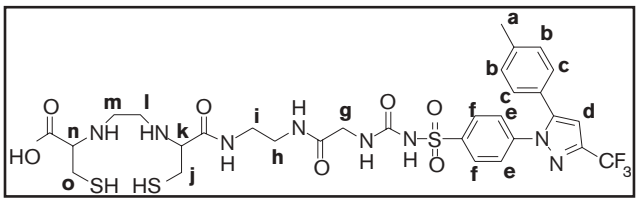

Observed (p.p.m.)

7.80 (2H, d, *J*=8.6Hz)	**f**
7.33 (2H, d, *J*=8.6Hz)	**e**
7.01–7.11 (4H, m)	**c,b**
6.90 (1H, s)	**d**
4.15 (2H, s)	**g**
3.55–3.65 (2H, m)	**k, n**
3.43–3.53 (4H, m)	**h, i**
2.99 (2H, d, *J*=7.0Hz)	**j**
2.94 (2H, d, *J*=9.0Hz)	**o**
2.41 (4H, d, *J*=3.0Hz)	**l, m**
2.16 (3H, s)	**a**

^{1}H-NMR spectra data of EC–CBX.

room temperature with horseradish peroxidase-labeled anti-mouse secondary antibody (Amersham Life Science, Arlington Heights, IL), signals were detected by the enhanced chemiluminescence assay (Amersham Life Science) according to the manufacturer's instructions.

Three cancer cell lines (13762, A549 and H226) with different COX-2 expression and activities were used to study the effect of cellular uptake after CBX induction at various doses. All cell lines were maintained in culture with Dulbecco's modified Eagle medium supplemented with 10% fetal calf serum, glutamine and antibiotics, in a humidified atmosphere with 5% CO_2 and 95% air. The cells were treated with celebrex (0.25–5 mg/well) for 30 min, followed by adding 4 μCi (0.148 MBq) of ^{99m}Tc-EC–CBX (0.1 mg/well) to each well. Cells were incubated with radiotracers at 37°C at 0.5–4 h. After incubation, cells were washed with ice-cold phosphate-buffered saline (PBS) twice and trypsinized with 0.5 ml of trypsin solution. Then cells were collected and the radioactivity was measured by a γ-counter. Data are expressed in mean ± SD percent uptake ratio of three measurements.

In vivo biodistribution and dosimetry of ^{99m}Tc-EC–CBX in tumor-bearing rats

The animal experiments were approved by the University of Texas M. D. Anderson Institutional Animal Care and Use Committee. Female Fischer 344 rats (150 ± 25 g) (Harlan Sprague-Dawley, Indianapolis, IN) were inoculated s.c. with 0.1 ml of mammary tumor cells from the 13762 tumor cell line suspension (10^6 cells/rat, a tumor cell line specific to Fischer rats) into the hind legs using 25-gauge needles. Studies were performed 14–17 days after implantation when tumors reached approximately

1 cm in diameter. Rats were anesthetized with ketamine (10–15 mg/rat, i.p.) before each procedure. Each animal was injected i.v. with 370–550 kBq of ^{99m}Tc-EC–CBX or ^{99m}Tc-EC ($n = 3$/time point). The injected mass of ^{99m}Tc-EC–CBX was 100 µg per rat. At 0.5, 2 and 4 h following administration of the radiotracers, the rats were sacrificed and the selected tissues were excised, weighed and counted for radioactivity by using a γ-counter (Packard Instruments, Downers Grove, IL). The biodistribution of tracer in each sample was calculated as percentage of the injected dose per gram of tissue wet weight (%ID/g). Tumor/non-tumor tissue count density ratios were calculated from the corresponding %ID/g values. Student's *t*-test was used to assess the significance of differences between groups.

Dosimetric calculations were performed using in-house curve-fitting software. Time–activity curves were generated for each organ. Analytic integration of the curves was used to determine the area under the curve (AUC) which was then divided by injected dose to yield the residence time of each organ. Residence times were then used to calculate target organ absorbed radiation doses based on the MIRD methodology for the normal adult male using the MIRDose 3.1 soft ware package [24].

Scintigraphic imaging studies

Scintigraphic imaging studies was performed in rats and rabbits animal models. For rats, female Fischer 344 rats (150 ± 25 g) (Harlan Sprague-Dawley, Indianapolis, IN) were inoculated s.c. with 0.1 ml of mammary tumor cells from the 13762 tumor cell line suspension (10^6 cells/rat, a tumor cell line specific to Fischer rats) into the hind legs. For rabbits, New Zealand white rabbits were inoculated with VX-2 tumor mass (rabbit-driven squamaceous mammary tumor). For mice, athymic nude mice were inoculated s.c. with 0.1 ml of tumor cells from the A549 and H226 tumor cell line suspension (2×10^6 cells/mouse) into the hind legs. Studies performed 12–17 days after implantation when tumors reached approximately 1 cm in diameter. The animals were administered with ^{99m}Tc-EC–CBX or ^{99m}Tc-EC (0.3 mCi/rat; 1 mCi/rabbit, 0.1 mCi/mouse, $n = 3$, i.v.) and the scintigraphic images, using a γ camera equipped with a low-energy, parallel-hole collimator, were obtained at 0.5–4 h after i.v. injection of the radiotracers. To assess locoregional radioactivity, a small hand-held γ camera (eZ-SCOPE; Anzai Medical, Tokyo, Japan) was also used with a low-energy parallel-hole collimator (high sensitive type). The field of view for eZ-SCOPE is 32 mm × 32 mm with 16 × 16 pixels, of which the intrinsic spatial resolution is 2 mm and sensitivity is 770 000 c.p.s./MBq. To demonstrate whether inducible COX-2 expression could be imaged by ^{99m}Tc-EC–CBX, a group of nude mice bearing human lung tumors (A549 and H226) was pretreated with CBX (1 mg, i.p.) and the images were acquired at 2 h after i.v. injection of ^{99m}Tc-EC–CBX. Computer-outlined regions of interest (ROI) (counts per pixel) of the tumor lesion site and symmetric normal muscle site were used to determine tumor:background count density ratios. The ratios were used to compare dynamic tumor uptake pre- and post-treatment of CBX.

Acute toxicity studies

Swiss-Webster mice (17-20 g, male and female, 12 each) were purchased from Harlan Sprague-Dawley (Indianapolis, IN) and housed at all times in animal rooms in the M. D. Anderson Cancer Center with controlled temperature (21–23°C), humidity (50–55%) and light period (on at 0600 h, off at 1800 h). Following 2 control days, mice were administered an i.v. injection (tail vein) of saline and EC–CBX (20, 40 and 100 mg/kg) ($n = 3$/dosage), and body weight was measured daily. Control groups were administered saline only. EC–CBX (5 mg) was dissolved in 1 ml of water. The final concentration used for animal studies was 5 mg/ml. The injection volume was 0.08–0.4 ml per mouse.

Results

In vitro cellular uptake studies

Western blot analysis indicated that 13762 and A549 cancer cells showed positive COX-2 expression (Fig. 5). There was a significant increase in uptake after pretreating cells with CBX. At higher dose (5 mg CBX/well), the uptake was decreased. The findings suggest COX-2 enzyme might be induced by pretreatment with CBX (Figs 6–8). In addition, higher COX-2 expression cell lines (A549 and 13762) had higher uptake than lower COX-2 expression cell line (H226) [22].

Biodistribution and dosimetric estimates

Biodistribution of ^{99m}Tc-EC–CBX in tumor-bearing rats showed increased tumor:tissue count density ratios as a function of time compared to ^{99m}Tc-EC (Tables 1 and 2). Based upon preclinical biodistribution studies, dosimetry was estimated from MIRDose (Table 3). If the subject does not involve other radiation exposure, whole-body, liver and effective dose equivalent for the proposed single

Fig. 5

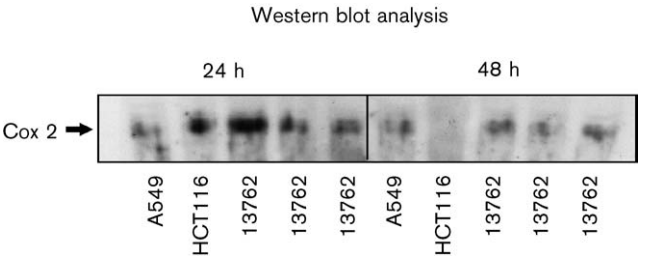

Western immunoblotting assays indicated that A549 and 13762 cells showed positive COX-2 expression.

Fig. 6

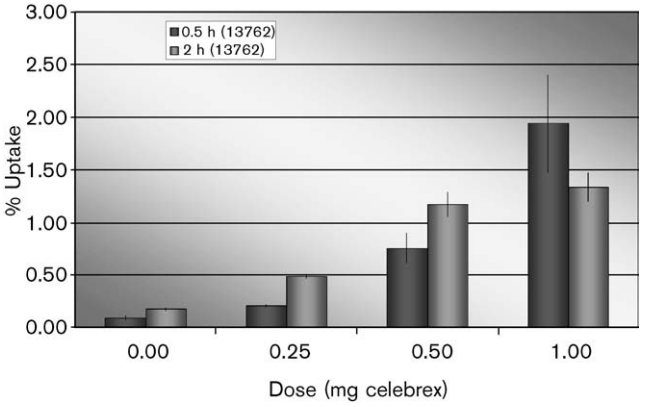

In vitro cellular uptake assays of ^{99m}Tc-EC–CBX in the 13762 cell line (high COX-2 expression) showed that cells pretreated with CBX had an increased uptake of ^{99m}Tc-EC–CBX.

Fig. 7

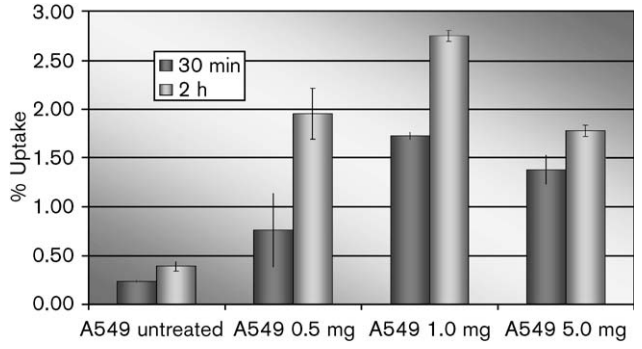

In vitro cellular uptake assays of ^{99m}Tc-EC–CBX in the A549 cell line (medium COX-2 expression) showed that cells pretreated with CBX had an increased uptake of ^{99m}Tc-EC–CBX.

dose at 30 mCi are less than 0.103, 1.5 and 0.375 rad, which should fall below the limits for 3 rem annual and 5 rem total dose equivalent, and other organs of single dose at 5 rem annual and total dose equivalent at 15 rem. Subjects should not be enrolled in this protocol if they have participated in another research protocol involving ionizing radiation within the past year.

Gamma scintigraphic imaging of ^{99m}Tc-EC–CBX in tumor-bearing animal models

Planar images of tumor-bearing animal models confirmed that the tumors could be visualized clearly with ^{99m}Tc-EC–CBX (Figs 9–11), whereas less tumor uptake in the ^{99m}Tc-EC group was observed (Fig. 12). Computer-outlined ROI showed that the tumor:background ratios in ^{99m}Tc-EC–CBX group were significantly higher than

Fig. 8

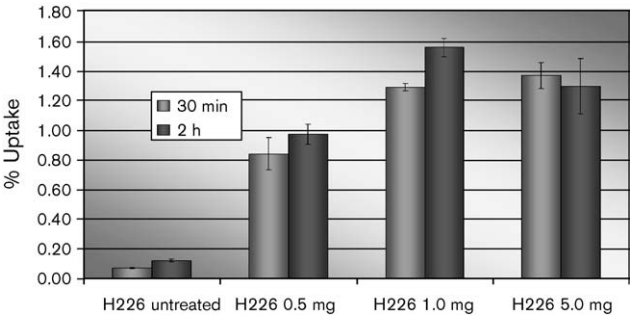

In vitro cellular uptake assays of ^{99m}Tc-EC–CBX in the H226 cell line (low COX-2 expression) showed that cells pretreated with CBX had an increased uptake of ^{99m}Tc-EC–CBX. However, the magnitude of uptake was less than for A549 and 13762 cells.

those in the ^{99m}Tc-EC group. The optimal imaging time was 2 h in a rabbit model. In a mouse model, pretreatment with CBX showed an increased tumor uptake with ^{99m}Tc-EC–CBX in the A549 model compared to the H226 model (Fig. 9). This increased tumor uptake might be due to COX-2 enzyme induced by CBX at low dose.

Acute toxicity studies

At the dosage of 100 mg/kg, all mice died. At the dosage of 20–40 mg/kg, all mice were alive and tolerated the doses well. The mice were observed for 4 days. No changes in body weight were seen. In humans, we plan to use 1.5 mg per 70 kg patient (25–29 mCi). The dose range selected is 1000–2000 times higher than the human dose.

Discussion

Assessment of the effectiveness of cancer therapy (e.g. volumetric and morphological changes) is usually measured by computed tomography and magnetic resonance imaging. In addition to these imaging modalities, the treatment endpoints rely almost exclusively on the analysis of biopsies by molecular and histopathological methods. These methods provide a microscopic picture of the general heterogeneous process. Therefore, to assess clinical endpoints adequately, a functional cellular marker is needed that would allow precise, spatio-temporal measurement of tumor targets on a whole-body image upon administration of a functional agent. These mechanism-based agents provide image-guided therapy which may discontinue ineffective treatment in the earlier phase and be beneficial to patients.

PET and SPECT use radiotracers to image, map and measure target site activities (e.g. angiogenesis, metabo-

Table 1 Biodistribution of ^{99m}Tc-EC in breast tumor-bearing rats (% of injected dose per gram of tissue weight)

	30 min	1 h	2 h	4 h
Blood	0.44 ± 0.03	0.27 ± 0.04	0.21 ± 0.00	0.15 ± 0.01
Lung	0.27 ± 0.02	0.19 ± 0.03	0.14 ± 0.00	0.12 ± 0.01
Liver	0.51 ± 0.06	0.367 ± 0.01	0.29 ± 0.07	0.23 ± 0.02
Spleen	0.12 ± 0.01	0.09 ± 0.00	0.08 ± 0.00	0.07 ± 0.00
Stomach	0.14 ± 0.06	0.13 ± 0.11	0.04 ± 0.03	0.04 ± 0.01
Kidney	7.91 ± 0.90	8.99 ± 0.27	9.12 ± 0.05	7.83 ± 1.02
Thyroid	0.22 ± 0.04	0.23 ± 0.12	0.11 ± 0.00	0.08 ± 0.01
Muscle	0.06 ± 0.01	0.04 ± 0.00	0.03 ± 0.01	0.02 ± 0.00
Intestine	0.17 ± 0.03	0.79 ± 0.11	0.40 ± 0.09	0.10 ± 0.01
Urine	9.12 ± 0.81	11.05 ± 6.16	13.19 ± 4.51	8.69 ± 2.98
Tumor	0.34 ± 0.16	0.15 ± 0.02	0.12 ± 0.00	0.10 ± 0.01
Tumor/blood	0.78 ± 0.32	0.54 ± 0.00	0.55 ± 0.01	0.65 ± 0.01
Tumor/muscle	5.84 ± 3.25	3.41 ± 0.33	4.43 ± 1.34	5.09 ± 0.22
Tumor/lung	1.26 ± 0.43	0.80 ± 0.02	0.80 ± 0.00	0.80 ± 0.01

Values shown represent the mean ± SD.

Table 2 Biodistribution of ^{99m}Tc-EC–CBX in breast tumor-bearing rats (% of injected dose per gram of tissue weight (n = 3/time, interval, i.v.)

	30 min	2 h	4 h
Blood	2.293 ± 0.038	1.388 ± 0.063	1.031 ± 0.033
Heart	0.475 ± 0.025	0.283 ± 0.017	0.224 ± 0.004
Lung	1.033 ± 0.035	0.712 ± 0.098	0.500 ± 0.011
Liver	1.556 ± 0.046	1.461 ± 0.049	1.506 ± 0.080
Spleen	0.594 ± 0.298	0.965 ± 0.056	0.981 ± 0.041
Kidney	4.963 ± 0.147	6.088 ± 0.305	6.363 ± 0.260
Intestine	0.406 ± 0.039	0.276 ± 0.061	0.190 ± 0.006
Uterus	0.595 ± 0.003	0.334 ± 0.034	0.263 ± 0.005
Muscle	0.133 ± 0.007	0.062 ± 0.003	0.002 ± 0.004
Tumor	0.587 ± 0.062	0.424 ± 0.019	0.406 ± 0.004
Thyroid	0.784 ± 0.090	0.449 ± 0.015	0.372 ± 0.021
Stomach	0.370 ± 0.010	0.187 ± 0.004	0.139 ± 0.004
Bone and joint	0.324 ± 0.036	0.190 ± 0.003	0.178 ± 0.022
Tumor/muscle	4.375 ± 0.304	6.876 ± 0.704	9.715 ± 0.387
Tumor/blood	0.255 ± 0.022	0.307 ± 0.018	0.395 ± 0.014
Uterus/blood	0.259 ± 0.003	0.240 ± 0.021	0.255 ± 0.005
Uterus/muscle	4.471 ± 0.257	5.442 ± 0.852	6.278 ± 0.199
Bone/muscle	2.419 ± 0.225	3.058 ± 0.114	4.314 ± 0.739

Values shown represent the mean ± SD of data from three animals.

Table 3 Radiation dose estimates of ^{99m}Tc-EC–CBX for the reference adult

Target organ	Total dose[a]	
	mGy/MBq	rad/mCi
Adrenals	2.89E–03	1.07E–02
Brain	6.73E–06	2.49E–05
Breasts	3.65E–04	1.35E–03
Gallbladder wall	4.00E–03	1.48E–02
LLI wall	1.47E–04	5.43E–04
Small intestine	7.81E–04	2.89E–03
Stomach	1.17E–03	4.33E–03
ULI wall	1.06E–03	3.93E–03
Heart wall	1.46E–03	5.40E–03
Kidneys	2.08E–02	7.70E–02
Liver	1.30E–02	4.82E–02
Lungs	1.75E–03	6.47E–03
Muscle	4.82E–04	1.78E–03
Ovaries	2.58E–04	9.55E–04
Pancreas	2.59E–03	9.56E–03
Red marrow	6.15E–04	2.28E–03
Bone surfaces	7.86E–04	2.91E–03
Skin	2.13E–04	7.90E–04
Spleen	7.47E–03	2.76E–02
Testes	1.12E–05	4.13E–05
Thymus	3.73E–04	1.38E–03
Thyroid	1.76E–03	6.52E–03
Urinary bladder wall	7.41E–05	2.74E–04
Uterus	2.26E–04	8.36E–04
Total body	9.31E–04	3.44E–03
Effect dose equivalent (EDE)[b]	3.37E–03	1.25E–02
Effective dose (ED)[b]	1.94E–03	7.19E–03

[a]Residence times: heart contents 1.50E–02 h; kidneys 3.94E–01 h; liver 1.08E + 00 h; lungs 5.80E–02 h; spleen 7.40E–02 h; thyroid 3.00E–03 h.
[b]Units of EDE and ED are mSv/MBq or rem/mCi.

Fig. 9

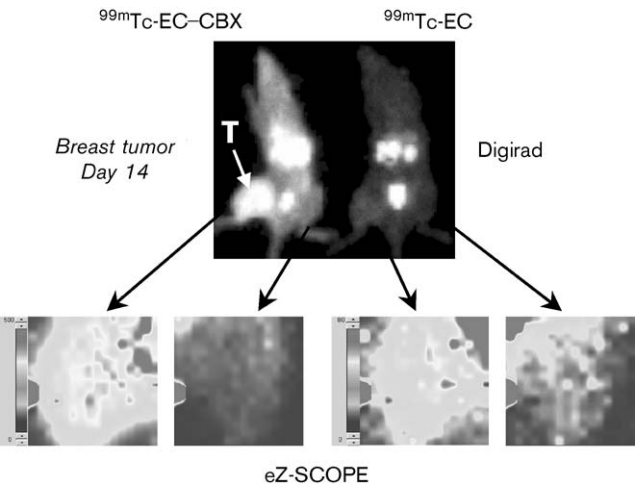

Anterior view of breast tumor-bearing rats receiving ^{99m}Tc-EC–CBX and ^{99m}Tc-EC (300 μCi, i.v.) showed that there was tumor uptake (T) at 2 h post-injection with ^{99m}Tc-EC–CBX.

lism, apoptosis and proliferation), and they are considered as molecular imaging modalities.

Reliable molecular imaging assays that assess (i) cellular targets at low cost, (ii) treatment response more rapidly, (iii) differential diagnosis, (iv) the prediction of therapeutic response and (v) better dosimetry for internal radiotherapy would be very valuable. Though FDG-PET imaging demonstrates the increased glucose consumption of malignant cells, problems with specificity for cell proliferation have led to the development of new PET tracers. [^{18}F]FDG could assess early metabolic activity, but it could not adequately assess cell translational activity. Thus, [^{18}F]FDG could not differentiate infection/inflammation versus tumor recurrence. To develop a tumor-specific agent it is necessary to assess both cellular and vascular activity. Assessment of cellular and vascular activity may provide potential applications in differential diagnosis and prediction of early treatment response.

COXs catalyze the synthesis of PGs from arachidonic acid. Overexpression of COX-2 is frequently found in human cancers and is suggested to play an important role in tumorigenesis. Recent studies indicated that COX-2

Fig. 10

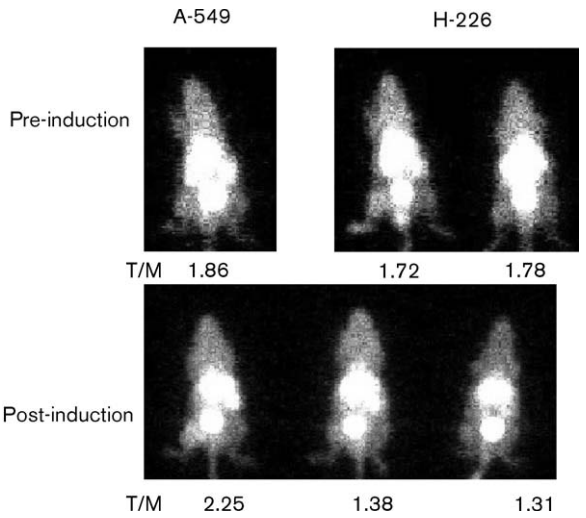

Anterior view of lung tumor-bearing mice receiving ^{99m}Tc-EC–CBX (300 μCi, i.v.) showed that there was slightly more tumor uptake in the A549 group compared to the H226 group post-treatment with CBX (1 mg, i.p.).

Fig. 11

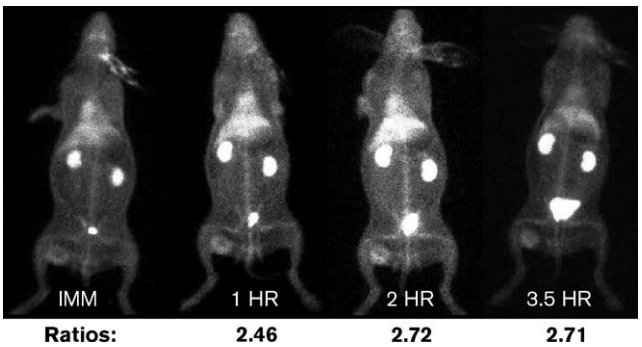

Computer-outlined ROI comparison of tumor:background ratios of ^{99m}Tc-EC–CBX in mammary tumor-bearing rabbits showed that optimal imaging time was 2 h post-injection.

Fig. 12

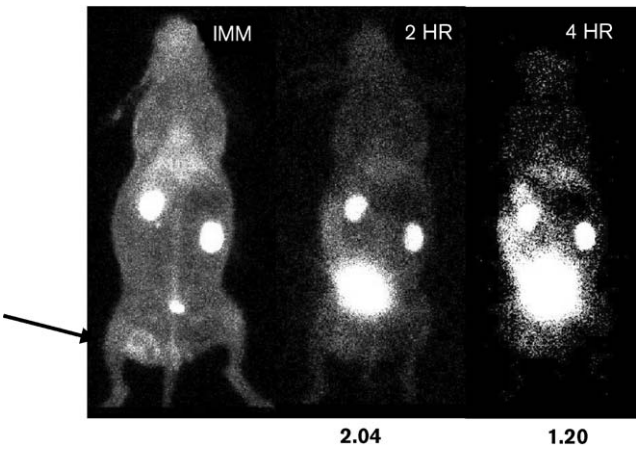

Computer-outlined ROI comparison of tumor:background ratios of ^{99m}Tc-EC in mammary tumor-bearing rabbits showed poor tumor uptake with time.

inhibitors exert potent anti-cancer effects on a number of cancers. Interestingly, some COX-2 inhibitors potently induce apoptosis, while other COX-2 inhibitors primarily induce growth inhibition. Therefore, there is a variability in the effects that different COX-2 inhibitors have on cancer cells [22,23]. Evidence from clinical and pre-clinical studies indicates that COX-2-derived PGs participate in carcinogenesis, inflammation, immune response suppression, apoptosis inhibition, angiogenesis, and tumor cell invasion and metastasis [25,26]. Clinical trial results have demonstrated that selective inhibition of COX-2 using high doses can alter the development and the progression of cancer [25]. Results of the current study indicated that COX-2 was an inducible enzyme when cells were treated with CBX at low dose. The findings suggest that an isozyme might be involved in cell lines expressing COX-2. Inhibition of this isozyme by CBX at low dose may induce COX-2 expression. This inducible COX-2 expression showed an increased uptake of ^{99m}Tc-EC–CBX. Others have shown a novel COX-1 splice variant termed COX-3. COX-3 is considered to play a key role in the biosynthesis of prostanoids known to be important mediators in pain and fever. Drugs that preferential block COX-1 also appear to act at COX-3. However, the existence of COX-3 at the nucleotide sequence level in humans has been called to question. A functional COX-3 in humans is still to come, underlining that the concept of COX-3 is still attractive [3,4,27–30].

In summary, EC–CBX can be labeled with ^{99m}Tc easily and efficiently, with high radiochemical purity and is cost-effective. *In vitro* cellular uptake and scintigraphic imaging studies demonstrated the pharmacokinetic distribution and feasibility of using ^{99m}Tc-labeled CBX to assess COX-2 expression of cancer. With complex mechanisms expressed in tumor tissue growth, the technique developed allows mechanism-specific targeted assessment of cell nuclei activity using ^{99m}Tc-EC–CBX. EC–CBX may also be chelated with other isotopes such as (^{68}Ga, ^{61}Cu) for PET imaging needs and ^{188}Re for internal radionuclide therapy.

Acknowledgments

The authors wish to thank Eloise Daigle for her secretarial support. This work was supported in part by

Cell > Point L.L.C. sponsored research grant (MDA LS01-212) and the John S. Dunn Foundation. The animal research and NMR facility are supported by the University of Texas M. D. Anderson Cancer Center (CORE) grant NIH CA-16672.

References

1 Bauer AK, Dwyer-Nield LD, Malkinson AM. High cyclooxygenase 1 (COX–1) and cyclooxygenase 2 (COX-2) contents in mouse lung tumors. *Carcinogenesis.* 2000; **21**:543–550.

2 Maihofner C, Probst-Cousin S, Bergmann M, Neuhuber W, Neundorfer B, Heuss D. Expression and localization of cyclooxygenase-1 and -2 in human sporadic amyotrophic lateral sclerosis. *Eur J Neurosci* 2003; **18**: 1527–1534.

3 Willoughby DA, Moore AR, Colville-Nash PR. COX-1, COX-2, and COX-3 and the future treatment of chronic inflammatory disease. *Lancet* 2000; **355**:646–648.

4 Botting R. COX-1 and COX-3 inhibitors. *Thromb Res* 2003; **110**:269–272.

5 Simmons DL. Variants of cyclooxygenase-1 and their roles in medicine. *Thromb Res* 2003; **110**:265–268.

6 Kawamori T, Wakabayashi K. COX-2 and prostanoid receptors: good targets for chemoprevention. *J Environ Pathol Toxicol Oncol* 2002; **21**:149–153.

7 Alshafie GA, Abou-Issa HM, Seibert K, Harris RE. Chemotherapeutic evaluation of Celecoxib, a cyclooxygenase-2 inhibitor, in a rat mammary tumor model. *Oncol Rep* 2000; **7**:1377–1381.

8 Davison A, Jones AG, Orvig C, Sohn M. A new class of oxotechnetium(+5) chelate complexes containing a $TcON_2S_2$ core. *Inorg Chem* 1981; **20**:1629–1632.

9 Verbruggen AM, Nosco DL, Van Nerom CG, Bormans GM, Adriaens PJ, *et al.* Tc-99m-L,L-ethylenedicysteine: a renal imaging agent. I. Labelling and evaluation in animals. *J Nucl Med* 1992; **33**:551–557.

10 Ratner S, Clarke HT. The action of formaldehyde upon cysteine. *J Am Chem Soc* 1937; **59**:200–206.

11 Blondeau P, Berse C, Gravel D. Dimerization of an intermediate during the sodium in liquid ammonia reduction of l-thiazolidine-4-carboxylic acid. *Can J Chem* 1967; **45**:49–52.

12 Van Nerom CG, Bormans GM, De Roo MJ, Verbruggen AM. First experience in healthy volunteers with Tc-99m-L,L-ethylenedicysteine, a new renal imaging agent. *Eur J Nucl Med* 1993; **20**:738–746.

13 Surma MJ, Wiewiora J, Liniecki J. Usefulness of Tc-99m-*N,N'*-ethylene-1-dicysteine complex for dynamic kidney investigations. *Nucl Med Commun* 1994; **15**:628–635.

14 Ilgan S, Yang DJ, Higuchi T, Zareneyrizi F, Bayhan H, Yu D, *et al.* ^{99m}Tc-ethylenedicysteine-folate: a new tumor imaging agent. Synthesis, labeling and evaluation in animals. *Cancer Biother Radiopharm* 1998; **13**:427–435.

15 Zareneyrizi F, Yang DJ, Oh CS, Ilgan S, Yu DF, Tansey W, *et al.* Synthesis of ^{99m}Tc-ethylenedicysteine–colchicine for evaluation of antiangiogenic effects. *Anticancer Drugs* 1999; **10**:685–692.

16 Yang DJ, Ilgan S, Higuchi T, Zareneyrizi F, Oh C-S, Liu C-W, *et al.* Noninvasive assessment of tumor hypoxia with ^{99m}Tc-labeled metronidazole. *Pharm Res* 1999; **16**:743–750.

17 Yang DJ, Azhdarinia A, Wu P, Yu D-F, Tansey W, Kohanim S, *et al.* *In vivo* and *in vitro* measurement of apoptosis in breast cancer cells using ^{99m}Tc-EC– Annexin V. *Cancer Biother Radiopharm* 2001; **16**:73–84.

18 Yang DJ, Kim K-D, Schechter NR, Yu D-F, Wu P, Azhdarinia A, *et al.* Assessment of antiangiogenic effect using ^{99m}Tc-EC–endostatin. *Cancer Biother Radiopharm* 2002; **17**:233–246.

19 Schechter NR, Yang DJ, Azhdarinia A, Kohanim S, Wendt 3rd R, Oh CS, *et al.* Assessment of epidermal growth factor receptor with ^{99m}Tc-ethylenedicysteine–C225 monoclonal antibody. *Anticancer Drugs* 2003; **14**:49–56.

20 Yang DJ, Kim CG, Schechter NR, Azhdarinia A, Yu DF, Oh CS, *et al.* Imaging with ^{99m}Tc ECDG targeted at the multifunctional glucose transport system: feasibility study with rodents. *Radiology* 2003; **226**:465–473.

21 Song HC, Bom HS, Cho KH, Kim BC, Seo JJ, *et al.* Prognostication of recovery in patients with acute ischemic stroke through the use of brain SPECT with ^{99m}Tc-labeled metronidazole. *Stroke* 2003; **34**:982–986.

22 Chang HC, Weng CF. Cyclooxygenase-2 level and culture conditions influence NS398-induced apoptosis and caspase activation in lung cancer cells. *Oncol Rep* 2001; **8**:1321–1325.

23 Liu W, Chen Y, Wang W, Keng P, Finkelstein J, Hu D, *et al.* Combination of radiation and celebrex (celecoxib) reduce mammary and lung tumor growth. *Am J Clin Oncol* 2003; **26**:S103–S109.

24 Stabin M. MIRDOSE: the personal computer software for use in internal dose assessment in nuclear medicine. *J Nucl Med* 1996; **37**:538–546.

25 Choy H, Milas L. Enhancing radiotherapy with cyclooxygenase-2 enzyme inhibitors: a rational advance?. *J Natl Cancer Inst* 2003; **95**: 1440–1452.

26 Gallo O, Franchi A, Magnelli L, Sardi I, Vannacci A, Boddi V, *et al.* Cyclooxygenase-2 pathway correlates with VEGF expression in head and neck cancer. Implications for tumor angiogenesis and metastasis. *Neoplasia* 2001; **3**:53–61.

27 Schwab JM, Schluesener HJ, Meyermann R, Serhan CN. COX-3 the enzyme and the concept: steps towards highly specialized pathways and precision therapeutics? *Prostaglandins Leukot Essent Fatty Acids* 2003; **69**: 339–343.

28 Botting RM. Mechanism of action of acetaminophen: is there a cyclooxygenase 3? *Clin Infect Dis* 2000; **31**:S202–S210.

29 Schwab JM, Schluesener HJ, Laufer S. COX-3: just another COX or the solitary elusive target of paracetamol? *Lancet* 2003; **361**:981–982.

30 Warner TD, Mitchell JA. Cyclooxygenase-3 (COX-3): filling in the gaps toward a COX continuum? *Proc Natl Acad Sci USA* 2002; **99**:13371–13373.